11th ANKARA INTERNATIONAL AEROSPACE CONFERENCE **AIAC-2021-012**
8-10 September 2021 - METU, Ankara TURKEY

NUMERICAL ANALYSIS OF FLOW CHARACTERISTICS AND VORTEX BREAKDOWN OF DIAMOND WING AT HIGH ANGLES OF ATTACK

Mustafa Murat Yavuz[1]
Izmir Democracy University
Izmir, Turkey

ABSTRACT

The relation between vortex breakdown and stall is mentioned in literature and it is a critical issue especially for unmanned combat air vehicles. The most effective source of vortex formation and breakdown is angle of attack and related studies are available, but they are examined in a limited angle of attack range. In this study, the effect of angle of attack on vortex formation and vortex breakdown of a diamond wing is investigated by using computational fluid dynamic analysis. The numerical analysis method was compared with experimental results before and the accuracy of the method was determined. Solutions were made at a constant Reynolds number of 10.000. Results of high angles of attack of wing are given up to 45^0 which are not available in literature. It is detected that flow disturbance begins at the lowest angle of attack. Beginning of vortex breakdown is detected at the angle of attack of 17^0 and it nearly reaches to front of the wing when angle of attack is equal to 25^0. Great eddies begin to form at the backside of the wing at the angle of attack of 30^0. Further increment of angle of attack causes to disturb flow characteristics. Rounding the leading edges is applied for decreasing vorticity. Streamline, particle injection and iso-value visualization results are given, and they are discussed in detail.

INTRODUCTION

Formation of vortices has been investigated for a long time. In literature different types and stages of vortex formations [Narayan and Seshadri, 1997] are mentioned that cause [Jacquin, 2005] instabilities. Formation of vortices is mainly categorized in three major groups from initial to last stage; initial flow disturbance, vortex formation and vortex breakdown.

Vortex breakdown [Lucca-negro and Doherty, 2001] is an important phenomenon, especially for combat air vehicles. Vortex breakdown [Lu and Zhu, 2004; Gursul et al., 2005; Kyriakou et al., 2010] occurs with sudden expansion of leading-edge vortices at the specified critical angle of attack including width range of flow separations [Sheta and Huttsell, 2003; Yayla et al., 2013]. Flow regime [Boelens, 2012] becomes complicated and strong reversed flow [Shan et al., 2005; Dang and Yang, 2010] is observed in those regions. Turbulent intensity [Breitsamter, 2008] increases rapidly and a part of flow energy [Cambier and Kroll, 2008] is transmitted to vortices. Critical value of angle of attack is determined with the location of vortex breakdown around the wing. Even if angle of attack [Schütte and Lüdeke, 2013] is increased a little, position of vortices moves to upstream. When vortex breakdown [Sheta and Huttsell, 2003;

[1] Assist. Prof. Dr. in Mechanical Engineering Department, Email: murat.yavuz@idu.edu.tr

Gordnier and Visbal, 2004] reaches to front of the wing, stall condition occurs. However, these theories [Nelson and Pelletier, 2003] are not commonly accepted and new investigations are required for understanding vortex structure.

Unmanned combat air vehicles (UCAVs) have different geometrical shapes and are used in specific areas. Cockpit is not necessary in these vehicles. Delta wings are one of the simplest unmanned combat air vehicles, widely used and several studies are available [Dang and Yang, 2010; Attar and Gordnier, 2006; Gordnier and Visbal, 1998; Mary, 2003; Miller and Williamson, 1997; Cummings and Schütte, 2013; Fritz, 2013]. Particle image velocimetry (PIV) is frequently used on investigations of flow characteristic of delta wing by researchers in experimental studies. Kinds of vortices around the wing [Levinski, 2001; Sohn and Chang, 2010; Lambert and Gursul, 2004] are classified and their effects are investigated.

Prevention of vortices has been investigated in some studies. Geometrical modifications, application of perturbations and prevention of transmission between flow energy and vortex formations are mainly considered in literature. Perturbations [Yavuz et al., 2004] reduce the number of critical points of flow topology and decrease the magnitude of surface vorticity. Application of small amplitude perturbation [Srigrarom and Lewpiriyawong, 2007; Yanıktepe and Rockwell, 2005; Yanıktepe, 2006] on delta, diamond and lambda wings delays the breakdown in a limited range and eliminates [Elkhoury, 2004; Yilmaz and Rockwell, 2009] large scale separation zone along the wing at high angle of attack. But the breakdown condition [Goruney and Rockwell, 2009] is not fully prevented.

The studies are mainly focused on the effect of attack, but in a limited range. In this study, a diamond wing is investigated for observing the flow characteristics and vortex breakdown, especially for high angles of attack. Relation between vortex formation and the changes in flow characteristic is clarified.

Computational fluid dynamics (CFD), which is one of numerical analysis techniques, is used in the study. In next chapter, why CFD is used is mentioned and some basic information is given. In the modelling chapter, numerical model of the wing is explained. Results of particle injection streamline topology at section plane, iso-values of z-vorticity and velocity contours around wing are given and discussed in the result chapter. Also, the effect of rounding the leading edge for decreasing vorticity is given. Main findings are summarized in conclusions.

CFD AND TURBULENCE MODELS

Numerical methods and computational solutions enable the widespread use of numerical analysis in engineering applications. New researches can be rapidly investigated, if the numerical model and results are suitable and logical. It is not required to prepare an experimental setup in the analyses. Investigated model and conditions are represented by mathematical descriptions. These descriptions include differential equations, which obey equilibrium and energy laws. The solution carries on these differential equations.

Most of the engineering problems include independent variables, time dependent and complex properties. Exact solutions may not exist in some cases and numerical methods can be used in such case that include approximate solution. Computational fluid dynamics (CFD) is an alternative way to investigate flow characteristics around diamond wing. CFD has better performance than experimental studies in some cases in literature. Observing the reattachment of shear layer and vortex breakdown around the wings [Boelens, 2012] are more easily observed in CFD rather than experimental techniques, such as PIV and LDA (laser Doppler anemometry). For that reason, CFD is used in this study.

Reynolds number of 10.000 is used in the analyses with respect to the study [Yanıktepe and Rockwell, 2005; Yanıktepe, 2006] and turbulent flow regime is considered. Different turbulence models are available in literature and one of the best-known turbulence models, k-epsilon (k-ε) is used in the analyses, because of its accuracy in low Reynolds number turbulent flows. k-epsilon turbulence model [Hoffmann and Chiang, 2000] includes one algebraic equation and two partial differential equations. Partial differential equations are turbulent kinetic energy, k

(determines the energy in the turbulence) and turbulent dissipation rate, ε (determines the scale of turbulence).

Turbulent kinetic energy and dissipation rate can be written [Hoffmann and Chiang, 2000] in analytical form as;

$$k = \frac{1}{2}\left[\overline{u'^2} + \overline{v'^2} + \overline{w'^2}\right] \quad (1)$$

$$\varepsilon = \nu_t \overline{\left(\frac{\partial u_i'}{\partial x_j}\right) * \left(\frac{\partial u_i'}{\partial x_j}\right)} \quad (2)$$

where v_t is eddy viscosity, u is x-direction velocity, v is y-direction velocity and w is z-direction velocity. k-ε two equation model [Hoffmann and Chiang, 2000] involves turbulent kinetic equation (3) and dissipation rate equation (4);

$$\rho \frac{dk}{dt} = \frac{\partial}{\partial x_j}\left[\left(\mu + \frac{\mu_t}{\sigma_k}\right)\frac{\partial k}{\partial x_j}\right] + P_k - \rho\varepsilon \quad (3)$$

$$\rho \frac{d\varepsilon}{dt} = \frac{\partial}{\partial x_j}\left[\left(\mu + \frac{\mu_t}{\sigma_\varepsilon}\right)\frac{\partial \varepsilon}{\partial x_j}\right] + c_{\varepsilon 1} P_k \frac{\varepsilon}{k} - c_{\varepsilon 2}\,\rho \frac{\varepsilon^2}{k} \quad (4)$$

where μ is viscosity of fluid, μt is turbulent viscosity. P_k is production of turbulence and defined [Hoffmann and Chiang, 2000] as;

$$P_k = \tau_{ij}\left(\frac{\partial u_i}{\partial x_j}\right) \quad (5)$$

where τ_{ij} is viscous stresses and turbulent viscosity is related [Hoffmann and Chiang, 2000] to ε by;

$$\mu_t = \rho\, c_\mu \frac{k^2}{\varepsilon} \quad (6)$$

σ_k, σ_ε, $c_{\varepsilon 1}$, $c_{\varepsilon 2}$ and cμ are constants and they are equal to defaults values; 1.00, 1.30, 1.44, 1.92 and 0.09 respectively.

NUMERICAL MODELLING

A CFD model should be prepared with mesh/grid elements and its construction takes a long time to prepare. In literature the used number of mesh [Mary, 2003] is not effective, if enough number of elements is used in the numerical model. Also, difference between coarse and fine grid results [Cambier and Kroll, 2008] is small, which are compared with an experimental study. Sensitivity of used number of grid elements is investigated in the study of Gordnier and Visbal [Gordnier and Visbal, 1998] and similar results are achieved. CFD solution gives consistent results [Yavuz and Pınarbası, 2011] with compared experimental data about vortex breakdown around a delta wing.

Water channel and wing are modelled with the usage of optimum number of grid elements. More or less number of elements causes high computational cost or less accuracy. Hence optimum number of grid elements is used, and the results are compared with suitable experimental data in literature.

Models are constructed with solid modelling software and imported in CFD. Water channel geometry is demonstrated in Fig. 1, has a width of 927 mm, a depth of 610 mm and a length of 4928 mm. Front and back surface of the channel are determined as fluid inlet and outlet. Side surfaces are defined as walls. Wing is placed at the centre of channel and fixed with respect to angles of attack. Inlet turbulent intensity is selected as % 0.3, which is commonly used in the related studies [Yanıktepe and Rockwell, 2005; Yanıktepe, 2006; Elkhoury, 2004]. Water properties are used in the analyses, have a density of 1.000 kg/m^3 and a viscosity of 0.001003 kg/ms.

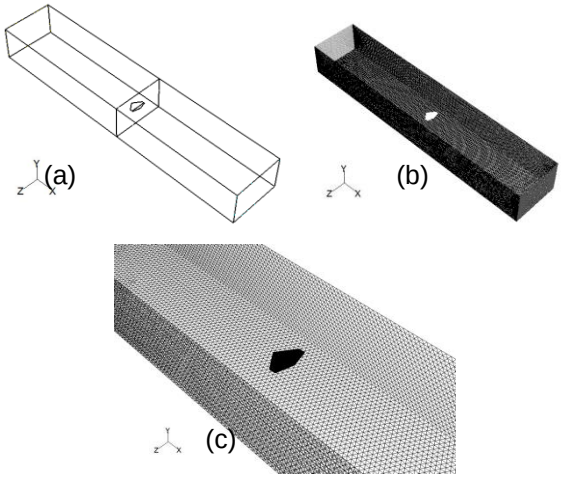

Figure 1: Numerical model of channel and wing; a) channel, wing location and section plane, b) numerical model of channel and wing, c) magnified view of channel inside and wing.

Observation of vortices around wing are carried out by particle injections in the flow. Particles have no mass and move directly with free-stream flow. They are injected from front of the wing. Approximately 20 to 30 particles are injected from injection location. Streamlines have been used to learn the behaviour of vortices around the wing and are observed from a specified section plane. Isometric and side view of section plane is shown in Fig. 2 and is placed at x/C=0.7, where x/C is the ratio of plane distance from front of the wing to total length of wing. The angle of attack (α) is illustrated in Fig. 2 and used as 7^0, 13^0, 17^0, 25^0, 30^0, 35^0, 40^0 and 45^0.

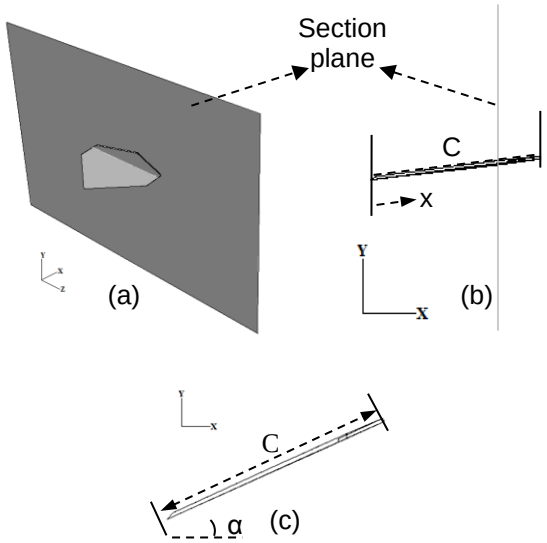

Figure 2: Section plane location on the wing, a) isometric view, b) side view, c) illustration of angle of attack

Model of diamond wing is given in Fig. 3. Numerical model of diamond wing and closer view of front location are given in Fig. 4. Diamond wing model has a width of 254 mm, chord length (C) of 195 mm and a thickness of 3 mm. Its leading edges are chamfered with an angle of 30^0 and edges are not rounded. Velocity of free-stream flow is determined as 51.4 mm/s based on a constant Reynolds number of 10.000 and chord length of diamond wing. Mapped meshing technique is used for setting number of elements on wing model. Approximately, 3.000.000 grid elements are used.

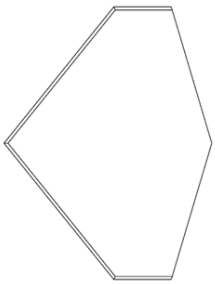

Figure 3: Analysed model of diamond wing.

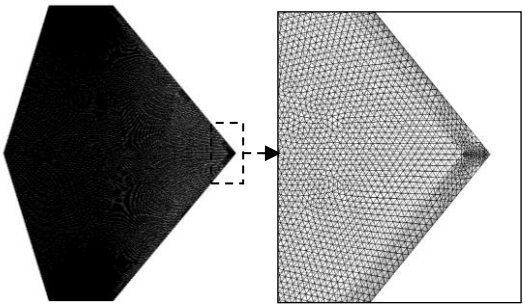

Figure 4: Numerical model of diamond wing geometry and closer view of front location.

NUMERICAL RESULTS AND DISCUSSION

Particle injection, streamline topology, velocity contours and iso-value results are given in the analyses. Initial case solutions are applied [Yavuz and Pınarbası, 2011; Yavuz, 2011] and compared with experimental results [Yanıktepe and Rockwell, 2005; Yanıktepe, 2006]. Similar streamline topology results are achieved between numerical and experimental results. More detail information can be achieved from the studies [Yavuz and Pınarbası, 2011].

Particle Injection Results

Dye injection in water channel is commonly used for observing flow characteristics of wings in experimental analyses. Similar observations are made by using particle injections in CFD analysis. Different particle materials and their injection properties are available. The used particles in this analysis have no mass and are injected in front of wing to free-stream direction. Some particles do not interact with vortices around wing and move freely. Interacted particles illustrate vortex formations and breakdown.

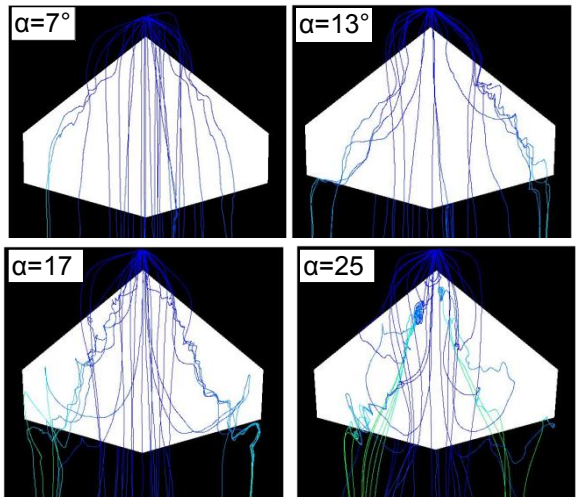

Figure 5: Particle injection results at low and moderate angles of attack (7^0, 13^0, 17^0, 25^0).

Particle injection results are given in Fig. 5 for low and moderate angles of attack. Vortices are observed from bottom view of the wing. Angle of attack solutions begin with 7^0. Even if angle of attack is small, disruption of particles is observed. Spiral vortex structures begin at this angle of attack. Small distortions occur nearly at x/C=0.3 and they move along with free stream until x/C=0.6. Two separated vortex arms occur, and they start moving away from each other to sides of wing. Increasing the angle of attack to 13^0 causes to form vortex structure evidently. Territory of vortex expands. Twisting of injected particles begin from x/C=0.3 and ends at end of the wing. Flow is disturbed from the wing tip when angle of attack is increased to 17^0. Two separated vortex structures come closer. Several particles twist widely and deflect at the rear of the wing. Reversed flow is observed at x/C=0.8 and it is an initial sign of vortex breakdown formation. Flow structure is impaired with increasing the angle of attack to 25^0. Twisting frequency increases and an accumulation location of particles has been detected at x/C=0.15. Reversed flow occurs at x/C=0.33 in left and at x/C=0.5 in right vortex arm. They are locations of vortex breakdown. Particles at the end of wing do not interact with backside edge of the wing. Without this trailing edge interaction, the flow does not expand sideways.

In Fig. 6, particle injection results of high angles of attack are given up to 45^0. When angle of attack is equal to 30^0, two separated vortex arms disappear in front of wing. A deposition location of particles occurs nearly at x/C=0.5 and then formation of two separated vortex arms is detected. Whole vortex structure occurs at the backside edge of the wing, when angle of attack is increased to 35^0. The separated vortex arms disappear. Due to multiple vortices occurring in a limited location, particle accumulation locations occur. Larger vortex structures are detected, and they are expanded towards the edges. They indicate the beginning of stall of plane. Vortex structure does not occur below the wing when angle of attack is equal to 40^0. Most of them are detected at the back and side locations of wing. Vortices get stronger and accumulate more. When angle of attack is equal to 45^0, Particle accumulation locations become larger and cover the entire rear of the wing. In this condition, wing acts like a flow barrier and flow regime around the wing changes critically.

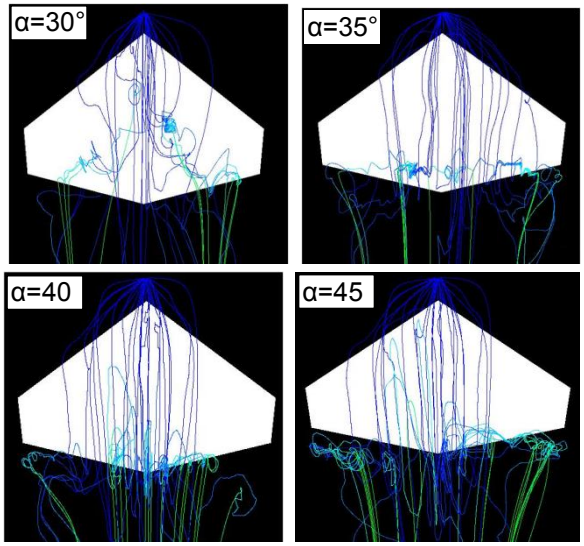

Figure 6: Particle injection results at high angles of attack (30^0, 35^0, 40^0, 45^0).

Side view of particle injection results is given in Fig. 7 for low and moderate angles of attack. Combination of this and bottom view illustrates more detail vortex formation. Initial disruptions are observed at angle of attack of 7^0. However, general form of flow around the wing is smooth. small disruptions are observed when angle of attack is increased to 13^0. It begins at x/C=0.3 and ends at approximately x/C=0.85. No flow separation still exists. As a result of angle of attack of 17^0, the vortex structure is observed. Vortices nearly begin in front of the wing and spiral particle flows are observed. Flow separation is detected at x/C=0.5. In later sections, a vortex flow begins and tries to move in the opposite direction of free stream flow. An expansion

is detected at x/C=0.76. Deposition locations are observed at x/C=0.1 and x/C=0.45 in the result of angle of attack of 25^0. Expansion of particles and direction changes are detected at x/C=0.42. Large swirls occur at the further locations of expansion. This location indicates formation of vortex breakdown.

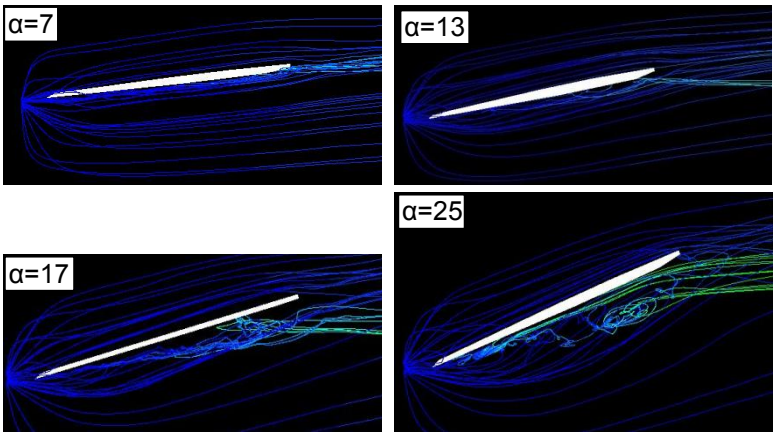

Figure 7: Side view of particle injection results at low and moderate angles of attack.

In Fig. 8, high angle attack results are given from the side view. When angle of attack is increased to 30^0, a great difference between upper and lower flows around the wing occurs. Swirls are detected at x/C=0.3 and back side. In the further sections, swirls move away from bottom surface of the wing. Deposition location of particles at the lower tip of the wing vanishes and it occurs at x/C=0.65. A great distance is observed between particles and the lower surface in the results of angle of attack of 35^0. Extremely distorted whirlpools are visible at x/C=0.6 and vortices move in the direction of free stream flow. Downstream flow increases swirls and their sizes below the wing in angle of attack of 40^0. Vortex core spreads towards the end of the wing with increasing the angle of attack to 45^0. The diameter of the vortex core is almost as large as the chord length of the wing.

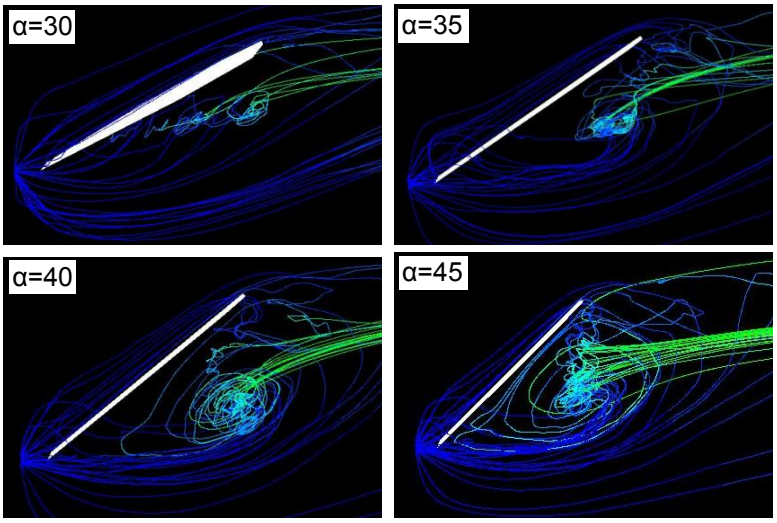

Figure 8: Side view of particle injection results at high angles of attack

Streamline Topology Results

Streamlines are another method used to show vortex formations and eddies around the wing. A section plane at x/C=0.7 is used to illustrate streamlines with respect to the studies [Yanıktepe and Rockwell, 2005; Yanıktepe, 2006]. Streamline results are given for half the wing.

Streamline topology is given in Fig. 9 for low and medium angles of attack. A swirl pattern is observed below the sharp corner of wing edge in the results of angle of attack of 7^0. Vortex core is small and smooth. A small vortex point is also detected, but not overpowering. When angle of attack is increased to 13^0, vortex point expands and enlarges. The vortex near the edge decreases. A new vortex point is detected at the lower surface of the wing. Only one vortex structure remains, and its expansion continues when angle of attack is equal to 17^0. In the results of 25^0, the vortex core rotates and continues to move towards the centre of the wing. Small free shear layers between vortex cores are observed in the results of 7^0 and 13^0.

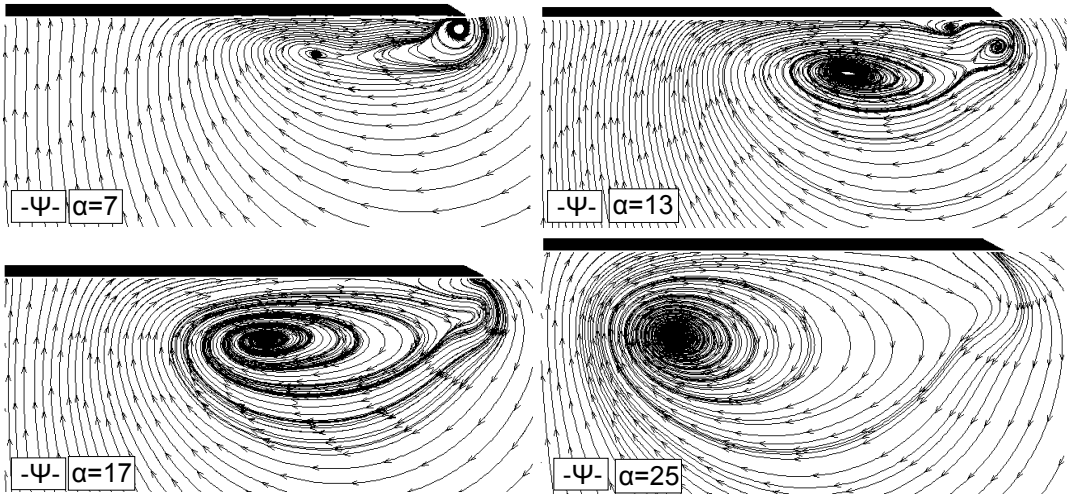

Figure 9: Streamline topology results at the x/C= 0.7 when angle of attack changes from 7^0 to 25^0.

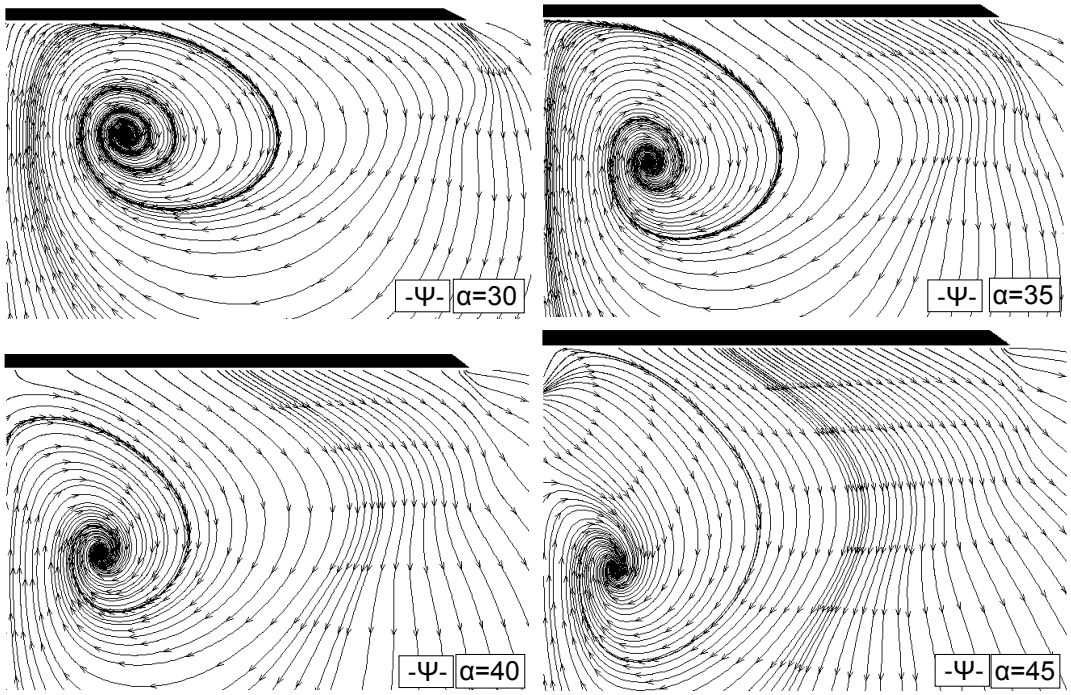

Figure 10: Streamline topology results at x/C= 0.7 when angle of attack changes from 30^0 to 45^0.

Streamline results of high angles of attack are given in Fig. 10. The rotation of the core becomes more circular and moves downward in a limited range, when angle of attack is increased from 30^0 to 40^0. The core has the closest location to the centre of the wing in the

result of 45^0. Streamlines which are interacted with below wing surface, are formed downwards.

Velocity Contours of Topology

The sudden expansion of vortex flows is a sign of vortex breakdown and various studies have been done in the literature to observe this condition. A relationship is mentioned between the size of vortex core and the stagnation pressure difference between the core and outer flow [Darmofal et al., 2001]. Therefore, it is convenient to control velocity contours and stagnation pressure locations around the wing.

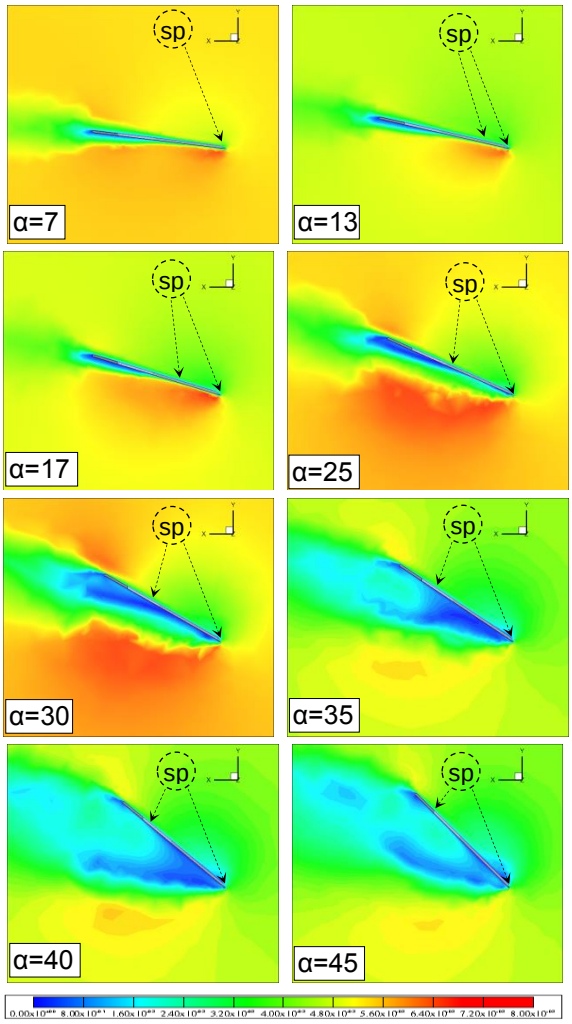

Figure 11: Velocity contours of diamond wing under different angles of attacks.

Velocity contours are given in Fig. 11 and results are taken from the side view of the wing by means of a centrally located plane parallel to the chord length. Stagnation points (sp) on the wing surfaces are given in the results, which is equal to one and indicates where the velocity is zero. As a result of the first angle of attack, one stagnation point is observed, while at the other angles two points are detected. One of the stagnation points occurs at the front edge of the wing in all cases. The result of first angle of attack (7^0) has only one stagnation point. When increasing the angle of attack to 13^0, two stagnation points occur. The second stagnation point is observed at the upper surface of wing at x/C=0.15. When angle of attack is increased to 17^0, the second stagnation point moves towards the end of the wing and occurs at x/C=0.3. The second stagnation point occurs at x/C=0.45 in the result of angle of attack of 25^0. It is detected at x/C=0.55 when angle of attack is increased to 30^0. When angle of attack is increased to 35^0,

40^0 and 45^0, second stagnation points occur at x/C=0.65, x/C=0.7 and x/C=0.8, respectively.

Velocity contours are given between 0 mm/s and 80 mm/s. A high velocity flow profile is observed at the below of wing. This profile extends almost to end of wing at the angle of attack of 7^0. When angle of attack (13^0 and 17^0) is increased, the size of the profile under the wing increases evenly. But, at the same time, a low velocity profile that forms under the wing end begins to spread. An expansion of low velocity profile begins at x/C=0.75 in the results of 17^0. When angle of attack is increased to 25^0, medium velocity profile forms below surface of the wing and push high velocity profile away from under the wing. High velocity profile expands rapidly, and two swirl locations are detected between x/C=0.2 and 0.4. The layer between high and medium velocity profile fluctuates. These are signs of vortex breakdown. Also, low velocity profile at the end of wing suddenly expands at the below of wing. Fluctuation of high velocity profile increases when angle of attack is increased to 30^0. Low velocity profile at the end of wing is separated from the below surface of wing and spreads backside. In the result of 35^0, high velocity profile vanishes around wing. The low velocity profile is completely separated from end and under surfaces and fluctuates in the results of 35^0 and 40^0. The intensity of the low velocity profile decreases at the highest angle of attack.

3D Mapping of Vorticity Field

Vortex formations can show basic vortex characteristics. Vortex formation occurs in 3 dimensions, which are x, y and z directions. Z-direction vortex is considered in this analysis, which clearly shows the effect of angle of attack. Z-vorticity value of 2 is used in demonstration of vortices and their locations are given in Fig. 12.

Vortices occur on the lower surface of the wing and cover almost the entire lower surface at the first angle of attack. When angle of attack increases (13^0, 17^0 and 25^0), three vortex regions occur; two of them spread sideways and the other spreads from front of wing to backside. These vortex spreads begin to decrease as the angle of attack increases. They mostly occur below the wing surface and begin to merge. When angle of attack is increased to 30^0, vortex spreads on the sides disappear. Similarly, the spread towards the middle of the wing is almost disappear. Vortices occur mostly on the side and front edges of the wing. They form as a cavity below the wing surface when the angle of attack is increased to the final angle of attack. The large vortex values become dominant and locations of z-vorticity value of 2 decrease.

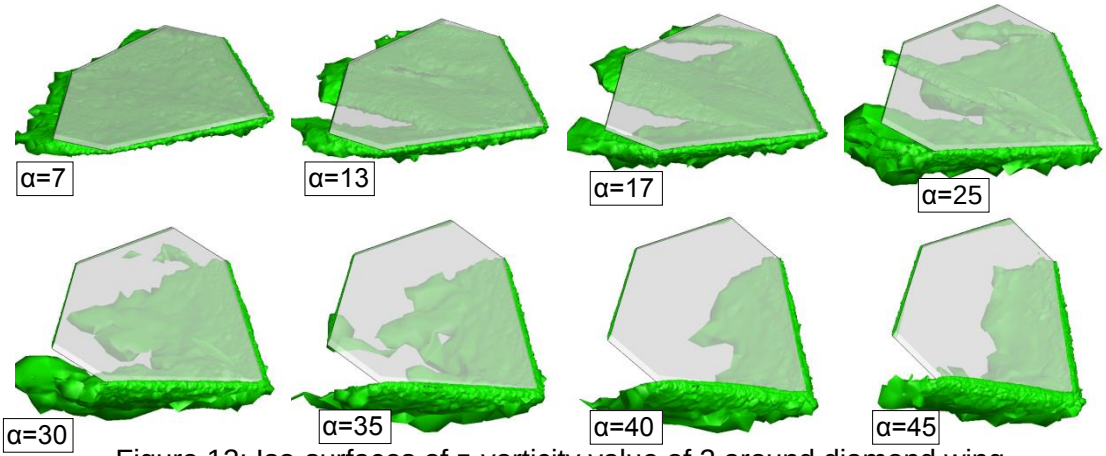

Figure 12: Iso-surfaces of z-vorticity value of 2 around diamond wing.

Effect of Fillet on Vorticity Values around Wings

Geometric shapes are the most critical design concepts in wings, and the initial design of the wings has low aerodynamic performance and requires development. Vortex formation can be reduced directly with appropriate modifications. Changing the wing aspect ratio [Yavuz, 2012], adding elliptical mounds [Yavuz, 2013a], or creating small circular grooves on the wing surfaces [Yavuz, 2013b] can control the formation of vortices in a limited range. However,

angle of attack on formation of vortices and vortex breakdown cannot be effectively eliminated. Therefore, new design concepts must be tried to prevent or delay vortex breakdown. The used wing geometry [Yanıktepe and Rockwell, 2005; Yanıktepe, 2006] has sharp corners and in general, sharp corners are known to increase flow separations. Sharp corners are often rounded to support smoother flow around the wings. Rounding the leading edges of a delta wing [Furman and Breitsamter, 2013] provides the flow separation to be delayed. Effect of rounding the leading edges can also be seen in the studies [Schütte and Lüdeke, 2013; Cummings and Schütte, 2013; Fritz, 2013].

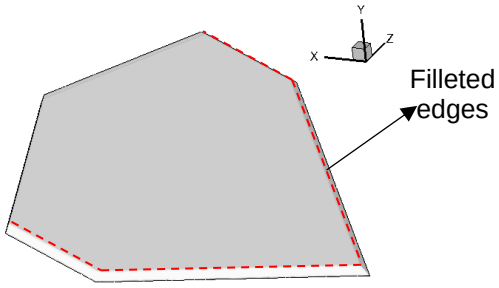

Figure 13: Illustration of filleted edges

Rounded edges are marked as red colour and shown in Fig. 13. Fillet radius and magnitudes of vortices are given in table 1. Dominant eddies occur in front of the wing and near the edges. Z-direction vortices have a dominant role on total vortices. Vortices are rapidly reduced according to the addition of rounding on the edges. High vorticity values occur in a small space resulting in high peak values. Rounding the marked edges with a radius of 3 mm directly reduces the total and z-direction vorticity values. Rounding radius of 6 mm and 9 mm results have lower vorticity values than the first unmodified solution. Increasing rounding radius decreases vorticity values at upper edges, but it increases the values at lower sharp edges. Almost all vortex peak values are reduced by the application of rounding.

Table 1. Effect of fillet on vorticity values

fillet radius	-z vorticity	+z vorticity	vorticity mag.
no fillet	-102.13	105.132	133.88
3 mm	-43.67	34.41	44.11
6 mm	-45.13	40.30	47.48
9 mm	-48.66	36.31	51.47

CONCLUSION

In this study, the diamond wing, one of the types of unmanned combat aircraft, is examined. Vortex formation is observed, and vortex breakdown is investigated according to different angles of attack. Angle of attack is used up to 45^0. Some of the findings of the study can be summarized as follows;

Flow disturbances begin at the first angle of attack and two eddies occur, starting at the wing tip and approaching the wing lateral edges. As the angle of attack increases, they begin to approach the wing centre and each other. Vortex structures are formed directly when angle of attack is equal to 13^0. Vortex breakdown is detected in the results of 17^0. Its location is approximately at x/C=0.76. Critical angle of attack is determined as 25^0, which causes vortex breakdown around the wing at x/C=0.42. High angles of attack cause large swirls and vortex structures. Vortex structures and core move down below the surface. A large vortex occurs at the highest angle of attack approximately equal to chord length of the wing. In some locations, particle accumulation locations are detected and disturb the flow regime.

Streamline topology results indicate that a vortex core forms below the wing edge surface. A small vortex point is detected. It expands under the wing and creates a new core. The edge core decreases. The new vortex core rotates and continues to move the centre of the wing. At high angles of attack, the core becomes more circular and moves downward. Free shear layers are observed in the results of 7^0 and 13^0.

Only one stagnation point is detected at the first angle of attack. Two stagnation points are observed in increments of the angle of attack. In all results, one of these occurs in front of the wing. The other occurs on the upper surface of the wing and moves to the rear with an increasing angle of attack. The velocity contours indicate that the high velocity profile widens and fluctuates with increasing angle of attack. The low velocity profile begins to cover the rear of the wing. The position of the vortices begins to move away from below the wing surface with increasing angle of attack in iso-value of 2 z-vorticity result. A geometric modification is applied by rounding the upper front edges of the wing. Vorticity values decrease with application of rounding in the results.

In all observations and findings, angle of attack can be increased up to 30^0 and it is difficult to maintain flight conditions in subsequent increases in angle of attack. In line with this study, new techniques should be investigated to prevent and delay vortex formation and breakdown, especially at high angles of attack.

References

Attar, P.J. and Gordnier, R.E. (2006) *Aeroelastic Prediction of the Limit Cycle Oscillations of a Cropped Delta Wing*, Journal of Fluids and Structures, Vol. 22, p: 45-58, 2006

Boelens, O.J. (2012) *CFD Analysis of the Flow Around the X-31 Aircraft at High Angle of Attack*, Aerospace Science and Technology, Vol. 20, p: 38–51, 2012

Breitsamter, C. (2008) *Unsteady Flow Phenomena Associated with Leading-Edge Vortices*, Progress in Aerospace Sciences, Vol. 44, p: 48–65, 2008

Cambier, L. and Kroll, N. (2008) *Miracle – a Joint Dlr/Onera Effort on Harmonization and Development of Industrial and Research Aerodynamic Computational Environment*, Aerospace Science and Technology, Vol. 12, p: 555-566, 2008

Cummings, R.M. and Schütte, A. (2013) *Detached-eddy Simulation of the Vortical Flow Field about the VFE-2 Delta Wing*, Aerospace Science and Technology, Vol. 24, p: 66–76, 2013

Dang, H. and Yang, Z. (2010) *Vortex Breakdown Over Delta Wing and Its Induced Turbulent Flow*, 2nd International Conference on Computer Engineering and Technology, Vol. 5, p: 473-477, 2010

Darmofal, D.L., Khan, R., Greitzer, E.M. and Tan, C.S. (2001) *Vortex Core Behaviour in Confined and Unconfined Geometries: A Quasi-One-Dimensional Model*, J. Fluid Mech., Vol. 449, p: 61-84, 2001

Elkhoury, M. (2004) *Aerodynamics of Unmanned Combat Air Vehicles: Flow Structure and Control*, Ph.D. Dissertation, Mechanical Engineering and Mechanics Dept. Pennsylvania: Lehigh University Press, 2004

Fritz, W. (2013) *Numerical simulation of the peculiar subsonic flow-field about the VFE-2 Delta Wing with Rounded Leading Edge*, Aerospace Science and Technology, Vol. 24, p: 45–55, 2013

Furman, A. and Breitsamter, C. (2013) *Turbulent and Unsteady Flow Characteristics of Delta Wing Vortex Systems*, Aerospace Science and Technology, Vol. 24, p: 32–44, 2013

Gordnier, R.E. and Visbal, M.R. (1998) *Numerical Simulation of Delta-Wing Roll*, Aerospace Science and Technology, Vol. 6, p: 341-351, 1998

Gordnier, R.E. and Visbal, M.R. (2004) *Computation of the aeroelastic response of a Flexible Delta Wing at High Angles of Attack*, Journal of Fluids and Structures, Vol. 19, p: 785-800, 2004

Goruney, T. and Rockwell, D. (2009) *Flow past a delta wing with a Sinusoidal Leading Edge: Near-Surface Topology and Flow Structure*, Exp Fluids, Vol. 47, p: 321-331, 2009

Gursul, I., Allan, M.R. and Badcock, K.J. (2005) *Opportunities for the Integrated Use of Measurements and Computations for the Understanding of Delta Wing Aerodynamics*, Aerospace Science and Technology, Vol. 9, p: 181–189, 2005

Hoffmann, K.A. and Chiang, S.T. (2000) *Computational Fluid Mechanics Volume III*, 4th ed. Engineering Education System, 2000

Jacquin, L. (2005) *On Trailing Vortices: A Short Review*, International Journal of Heat and Fluid Flow, Vol. 26, p: 843–854, 2005

Kyriakou, M., Missirlis, D. and Yakinthos, K. (2010) *Numerical Modeling of the Vortex Breakdown Phenomenon on a Delta Wing with Trailing-Edge Jet-Flap*, International Journal of Heat and Fluid Flow, Vol. 31, p: 1087–1095, 2010.

Lambert, C. and Gursul, I. (2004) *Characteristics of Fin Buffeting Over Delta Wings*, Journal of Fluids and Structures, Vol. 19, p: 307–319, 2004

Levinski, O. (2001) *Review of Vortex Methods for Simulation of Vortex Breakdown*, Australia: DSTO Aeronautical and Maritime Research Laboratory, 2001

Lu, Z. and Zhu, L. (2004) *Study on Forms of Vortex Breakdown Over Delta Wing*, Chinese Journal of Aeronautics, Vol. 17(1), p: 13-16, 2004

Lucca-negro, O. and Doherty, T. (2001) *Vortex Breakdown - A Review*, Progress in Energy and Combustion Science, Vol. 27, p: 431-481, 2001

Mary, I. (2003) *Large Eddy Simulation of Vortex Breakdown behind A Delta Wing*, International Journal of Heat and Fluid Flow, Vol. 24, p: 596–605, 2003

Miller, G.D. and Williamson, C.H.K. (1997) *Turbulent structures in the trailing vortex wake of A Delta Wing*, Experimental Thermal and Fluid Science, Vol. 14, p: 2-8, 1997

Narayan, K.Y. and Seshadri, S.N. (1997) *Types of Flow on the Lee Side of Delta Wings*, Prog. Aerospace Sci., Vol. 33, p: 167-257, 1997

Nelson, R.C. and Pelletier, A. (2003) *The Unsteady Aerodynamics of Slender Wings and Aircraft Undergoing Large Amplitude Maneuvers*, Progress in Aerospace Sciences, Vol. 39, p: 185–248, 2003

Schütte, A. and Lüdeke, H. (2013) *Numerical investigations on the VFE-2 65-degree Rounded Leading Edge Delta Wing Using The Unstructured DLR TAU-Code*, Aerospace Science and Technology, Vol. 24, p: 56–65, 2013

Shan, H., Jiang, L. and Liu, C. (2005) *Direct Numerical Simulation of Flow Separation around A Naca 0012 Airfoil*, Computers & Fluids, Vol. 34, p: 1096–1114, 2005

Sheta, E.F. and Huttsell, L.J. (2003) *Characteristics of F/A-18 Vertical Tail Buffeting*, Journal of Fluids and Structures, Vol. 17, p: 461–477, 2003

Sohn, M.H. and Chang, J.W. (2010) *Effect of A Centerbody on the Vortex Flow of a Double-Delta Wing with Leading Edge Extension*, Aerospace Science and Technology, Vol. 14, p: 11–18, 2010

Srigrarom, S. and Lewpiriyawong, N. (2007) *Controlled vortex breakdown on Modified Delta Wings*, Journal of Visualization, Vol. 10(3), p: 299-307, 2007

Yanıktepe, B. (2006) *Origin and Control of Vortex Breakdown of Unmanned Combat Air Vehicles*, Ph.D. Dissertation, Mechanical Engineering Dept. Adana- Çukurova University, 2006

Yanıktepe, B. and Rockwell, D. (2005) *Flow Structure on Diamond and Lambda Planforms Trailing Edge Region*, AIAA Journal, Vol. 43(7), p: 1490-1500, 2005

Yavuz, M.M. (2011) *Numerical Analysis of Vortex Breakdown of Unmanned Combat Air Vehicles*, M.Sc. Dissertation, Mechanical Engineering Dept. Adana: Cukurova University, 2011

Yavuz, M.M. (2012) *Investigation of effect of wing aspect ratio on Flow Characteristics Around Unmanned Combat Air Vehicle of X-45a Under Low Angles of Attack*, IV. National Aerospace Conference, Turkish Air Force Academy Press, (in Turkish), p: 1-18, 2012

Yavuz, M.M. (2013a) *Investigation of Effect of Formed Mound with Different Shapes and Heights on Formation of Vortices around A Delta Wing*, 2nd National Aeronautics Technology and Applications Conference, Ege University Press (in Turkish), p: 355-365, 2013a

Yavuz, M.M. (2013b) *Investigation of Effect of Opened Channels at the Upper Surface of Unmanned Combat Air Vehicle on Control of Vortices*, VII. National Aircraft Aviation and

Aerospace Engineering Congress. Chamber of Mechanical Engineering Press (in Turkish), p: 31-36, 2013b

Yavuz, M.M. and Pınarbası, A. (2011) *Investigation of Flow Characteristics and Vortex Breakdown of a Delta Wing*, 6th Ankara International Aerospace Conference, METU Press. p: 1-11, 2011

Yavuz, M.M., Elkhoury, M. and Rockwell, D. (2004) *Near-surface Topology and Flow Structure on A Delta Wing*, AIAA Journal, Vol. 42(2), p: 332-340, 2004

Yayla, S., Canpolat, C., Sahin, B. and Akilli, H. (2013) *The Effect of Angle of Attack on the Flow Structure over the Nonslender Lambda Wing*, Aerospace Science and Technology, Vol. 28, p: 417–430, 2013

Yilmaz, T.O. and Rockwell, D. (2009) Flow Structure on a Three-Dimensional Wing Subjected to Small Amplitude Perturbations, Exp Fluids, Vol. 47, p: 579-597, 2009